Highlights

On the optimization of vibration energy harvesting based on periodic and biperiodic structures

Shakiba Dowlati, Najib Kacem, Noureddine Bouhaddi

- Designing a biperiodic VEH to localize vibration energy in two frequency bandwidths
- Multi-objective optimization to improve periodic and biperiodic VEH performance
- Proof of concept and experimental validation on optimized periodic and biperiodic VEH

On the optimization of vibration energy harvesting based on periodic and biperiodic structures

Shakiba Dowlati*, Najib Kacem, Noureddine Bouhaddi

Université Marie et Louis Pasteur, CNRS, institut FEMTO-ST, Department of Applied Mechanics, 24 Rue de l'Épitaphe, Besançon, 25000, France

Abstract

This paper presents a comprehensive numerical and experimental investigation into the design optimization of electromagnetic vibration energy harvesting (VEH) devices. By leveraging periodic and biperiodic structures, the study exploits the energy localization phenomenon to enhance energy harvesting efficiency. Introducing optimal mistuning in a periodic structure allows vibration energy to be concentrated around specific mistuned zones, enabling targeted energy harvesting from these areas instead of the entire system. An optimization framework is developed to determine the optimal mistuning parameters, including the total number, magnitude, and locations of mistuned elements, with the goal of maximizing localized vibration energy. Initially, the optimization approach is applied to periodic harvesters with numerous subsystems. Building on these results, a biperiodic harvester is proposed to improve harvested power while effectively covering two distinct frequency bandwidths. The findings reveal that optimizing mistuning in approximately half of the subsystems can achieve 84% of the harvested power compared to fully periodic counterparts. To validate the methodology, an electromagnetic VEH device with eight weakly coupled subsystems is designed and fabricated. Experimental results, using the optimized mass mistuning derived from the optimization process, show excellent agreement with numerical predictions, achieving approximately 81% of total harvested power with only a 3% discrepancy. These results underscore the potential of periodic and biperiodic harvesters to significantly enhance harvested power and frequency bandwidth while reducing the number of transduction circuits, as well as the overall size and cost of the harvesters.

Keywords: Vibration energy harvesting, Period & biperiodic structures, Energy localization phenomenon, Multi-objective optimization

The increasing demand for renewable and sustainable energy sources has led to a significant interest in energy harvesting technologies. These technologies offer a promising alternative to conventional energy generation, reducing the environmental impacts of raw materials extraction for battery production [1]. In addition, the maintenance-free self-powered sensors provide crucial advantages in remote or harsh environments where regular battery replacement is impractical [2, 3]. Among various ambient energy sources, mechanical vibrations are abundant, reliable, and sustainable [4, 5]. Vibration energy harvesting (VEH) can be achieved using electromagnetic [6, 7], piezoelectric [8, 9], or triboelectric mechanisms [10, 11], with electromagnetic VEH being particularly attractive due to its high current and output power [12].

*Corresponding author (current address: LaMCoS, UMR CNRS 5259, INSA-Lyon, France)
Email address: shakiba.dowlati@insa-lyon.fr (Shakiba Dowlati)

Electromagnetic VEH based on linear resonant oscillators has shown efficiency only over a narrow frequency range, closely aligned with the harvester's resonant frequency [13, 14]. Introducing nonlinearities can make VEH devices more responsive to wider ranges of frequencies and amplitudes of vibration [15, 16, 17]. Nonlinearities can be introduced through material and geometric effects, such as those seen in Duffing oscillators, or via dynamic mechanisms like magnetic interactions [18, 19], magnetic levitation [20, 21], stretching strain in clamped resonators [22, 23], and impact-based systems [24, 25]. Various nonlinear techniques, such as frequency tuning [26, 27, 28], frequency up-conversion [29, 30], and multimodal systems [31, 32, 33, 34], have been explored to extend the operational range and efficiency of VEHs.

Ghasemi et al. [26] developed a comb resonator with adjustable resonant frequencies by combining mechanically softening and hardening springs, resulting in a wide range of tuning capabilities. Podder et. al. [35] incorporated repulsive magnetic tuning into a nonlinear MEMS electromagnetic VEH, enabling the adjustment of the system's nonlinear frequency response. Mahmoudi et. al. [36] proposed magnetic levitation for a multi-degree of freedom VEH, which combined the benefits of both modal interactions and magnetic nonlinearities. Yu et al. [37] designed a multimodal piezoelectric harvester that employs a beam connected to rotating shafts at its endpoints. The integration of hinged supports and rotating degrees of freedom lowered the first and third resonant frequencies.

Periodic structures, consisting of identical substructures arranged in a regular repeating pattern, fall under the category of multimodal systems. Weak structural irregularities in weakly coupled periodic structures can lead to the localization of free and forced vibrations [38, 39]. The extent of this localization depends on the coupling strength between identical substructures and the level of disorder. This phenomenon is known as normal mode localization, first discovered by Anderson in solid-state physics [40]. Mistuning, achieved by perturbing geometry, mass, or coupling stiffness, can significantly enhance energy localization [41, 42]. Several studies have employed the energy localization phenomenon in periodic multimodal structures for energy harvesting. Malaji and Ali [43] investigated the energy harvesting from a near-periodic structure using two mechanically coupled pendulums, showing that even slight mistuning can significantly increase vibration amplitude. Zergoune et al. [41] studied energy localization in a linear electromagnetic VEH using mass mistuning, demonstrating improvements in output power density. Aouali et. al. [44] investigated the energy localization phenomenon in a nonlinear quasi-periodic VEH device. Significant improvements in both frequency bandwidth and output power were observed compared to the case without mistuning. Biperiodic structures feature two alternating substructures with distinct properties (e.g., stiffness, mass, geometry), creating dual-frequency bandwidths [45]. To our knowledge, this concept remains unexplored for vibration energy harvesting in the literature.

Optimization techniques have become essential in addressing challenges related to structural design, material selection, and energy harvesting efficiency [46, 47, 48]. Huang et al. [49] optimized parameters such as wind speed and electromechanical coupling to maximize the voltage amplitude of energy harvesters subjected to galloping and base excitation. Gao et. al. [50] performed an optimization on the size and power output of a magnetic energy harvester. Aouali et. al. [47] optimized a quasi-periodic VEH with two and five oscillators with tunable nonlinearity and mode localization to enhance power output and frequency bandwidth. Dowlati et. al. [51, 52] performed a numerical design optimization on linear quasi-periodic VEH devices to enhance the maximum harvested power. However, to the best of the authors' knowledge, the optimization of large-scale VEH devices with periodic and biperiodic structures for maximiz-

ing harvested power and expanding frequency bandwidth has not been thoroughly investigated through both numerical and experimental studies.

In this paper, we propose the optimization of electromagnetic VEH devices based on weakly coupled periodic and biperiodic structures. The main idea is to maximize the harvested power while minimizing the number of mistuned subsystems by optimizing mass mistuning in terms of their number, magnitude, and location. An optimization procedure is developed for both periodic and biperiodic harvesters, enabling the exploration of mistuning effects through a Pareto front and establishing the correlation of optimal mistuning for large-scale systems with varying numbers of mistuned subsystems. Experimental validation of the optimization procedure is performed using a prototype VEH device with eight weakly coupled subsystems. The results demonstrate that optimal mistuning enhances harvested power, and for the biperiodic structure, also increases the bandwidth composed of multiple frequency bands.

1. Design and modeling

Fig. 1a illustrates the electromagnetic VEH device, which consists of N identical spiral-shaped springs, each coupled with neodymium (NdFeB) cylindrical magnets positioned at the center. The arrangement of these magnets generates a weak repulsive magnetic force between them, with the coupling strength adjustable by varying the distance between the magnets. The oscillators are connected to the electrical circuits via electromagnetic transduction. The relative motion between the magnet masses and coils induces a variation in the magnetic flux in the coil turns, generating an electrical current. This electrical energy is subsequently dissipated in load resistances.

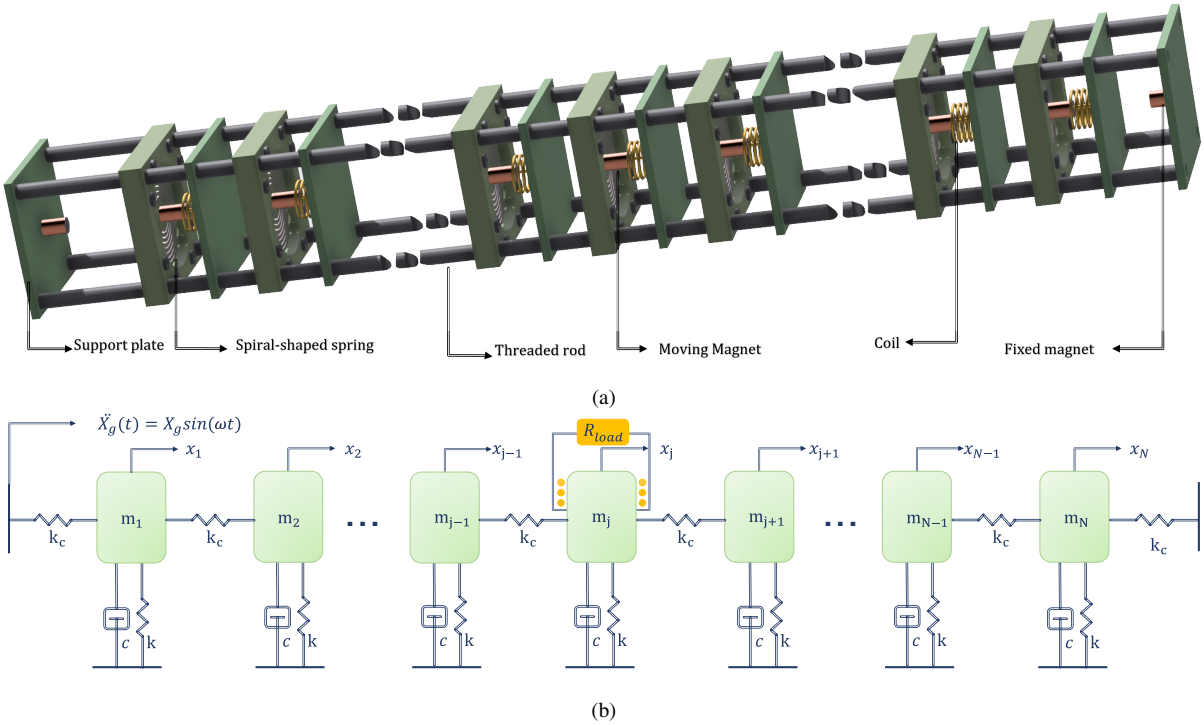

Figure 1: (a) Schematic diagram of the proposed electromagnetic VEH, consisting of N spiral-shaped springs with magnet masses at the center, each wrapped by wound copper coils, (b) The equivalent spring-mass-damper model of the proposed VEH device.

The proposed VEH device consists of repeated substructures, each with identical geometry, mass, damping, and stiffness coupling. Fig. 1b shows the coupled spring-mass-damper model of the proposed VEH device, with mass m, stiffness k, and viscous damping c. Each spring-mass-damper system is considered a subsystem, coupled to neighboring identical subsystems via coupling stiffness k_c. The system is subjected to base harmonic excitation $\ddot{X}_g$, with a constant amplitude X_g.

The governing equations of motion for the j^{th} subsystem, coupled by electromagnetic transduction, can be expressed as:

$$\begin{aligned} \ddot{x}_j + 2(\xi_m + \xi_e^j)\omega_0 \dot{x}_j + \alpha_j^{-1}\omega_0^2\left[(1+2\beta)x_j - \beta x_{j-1} - \beta x_{j+1}\right] &= -\ddot{X}_g \\ V_j + (R_{int} + R_{load}^j) i_j(t) &= 0, \\ V_j &= \delta_{em}\dot{x}_j, \\ i_j(t) &= \frac{\delta_{em}}{(R_{load}^j + R_{int})}\dot{x}_j, \end{aligned} \tag{1}$$

where ξ_m is the mechanical damping coefficient, ξ_e^j is the electrical damping coefficient of j^{th} subsystem, α_j is the ratio of the j^{th} mass to the initial mass m, δ_{em} is the electromechanical coupling coefficient, R_{int} and R_{load}^j are the internal resistance of the coil and the load resistance, respectively, β is the electromagnetic coupling coefficient, ω_0 is the undamped natural frequency of the system, and V_j and $i_j(t)$ are the induced voltage and current in the coils, respectively. Further details on the derivation of the governing equations of motion are provided in Appendix A.

The steady-state response of the harmonic excitation is given by $x_j = X_j \sin(\omega t - \phi)$. The instantaneous electrical power generated in the coil is $P_j(t) = c_e \dot{x}_j^2$, where $c_e = \frac{\delta_{em}^2}{(R_{load}^j + R_{int})}$ is the electrical damping [15]. The instantaneous harvested power is the power dissipated by the resistance in each energy harvesting circuit corresponding to each subsystem. Using Ohm's law, this power can be expressed as follows.

$$P_j(t) = R_{load}^j i_j^2(t). \tag{2}$$

The average load power harvested across the load resistances in all mistuned subsystems, over an oscillation cycle from t to $t + T$ is

$$P_{load}^j = \sum_{j=1}^{N} \frac{1}{2} R_{load}^j \left(\frac{\omega \delta_{em}}{(R_{load}^j + R_{int})} \right)^2 |X_j|^2. \tag{3}$$

1.1. Energy localization in quasi-periodic structures

Fig. 2a presents a periodic structure consisting of four weakly coupled spiral-shaped springs with proof masses at their centers, chosen as an example to illustrate the behavior of a multi-subsystem system. The spiral-shaped springs are designed, with their stiffness calculated calculated using ANSYS software [53] by applying a displacement at the center while fixing the outer boundary, and computing the stiffness as $k = F/\delta$, where F is the reaction force and δ is the displacement. The coupling between adjacent springs is achieved through 1D mechanical springs with weak stiffness, approximately 1.5% of the stiffness of the main spring. These 1D

springs model the magnetic repulsive interaction between successive subsystems. Numerical simulation is carried out to analyze the first modes of free vibration of the periodic structure shown in Fig. 2a. The first bending mode shape of the periodic structure is depicted in Fig. 2b, illustrating a uniform distribution of kinetic energy and consistent vibration amplitudes across the structure. Fig. 2c depicts the first bending mode shape of the structure subjected to variations in density. The mistuning is introduced by modifying the mass density of the second subsystem (counted from the top) by 5%, while leaving the rest of the system unchanged. This mass mistuning leads to the localization phenomenon, which effectively confines the global vibration energy to the mistuned subsystem. The subsystem with the mistuned mass density exhibits a significantly higher vibration amplitude compared to the other subsystems.

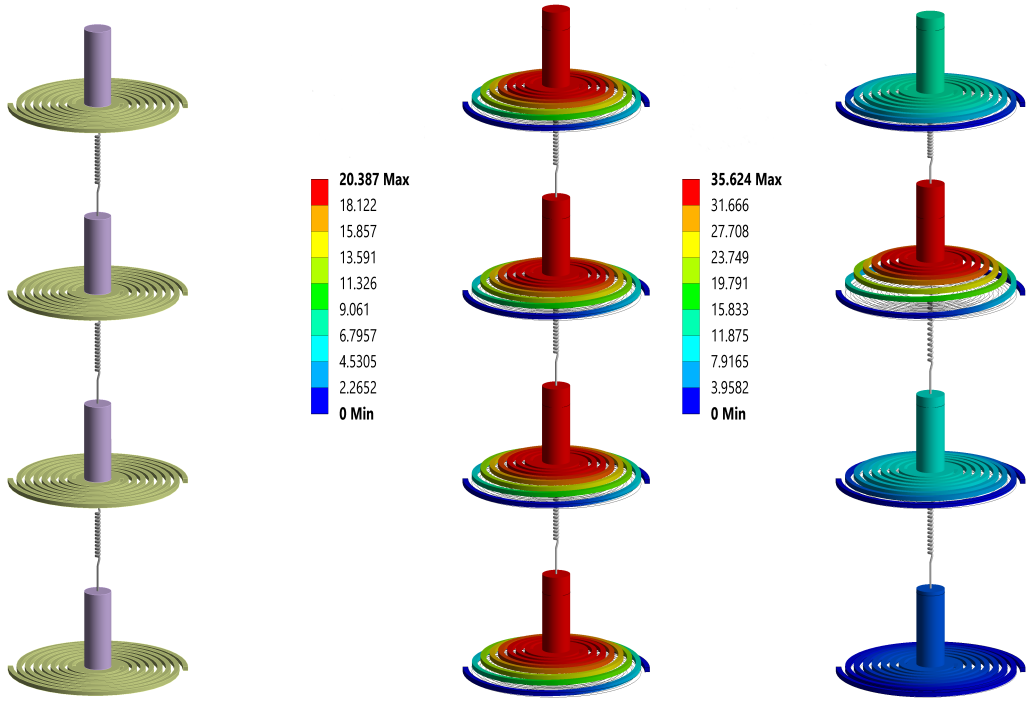

(a) (b) (c)

Figure 2: (a) A periodic structure of 4 weakly-coupled spiral-shaped springs with proof masses at the center, (b) The first bending mode shape of the periodic structure. (c) The first bending mode shape of the quasi-periodic structure with a variation of 5% in the mass density of the second spring (counted from the top). The color bar on the left-hand side of Fig. 2b and Fig. 2c corresponds to free vibration amplitudes.

1.2. Biperiodic structure

A biperiodic structure is a specific type of periodic arrangement consisting of two distinct types of substructures that are coupled together. The pattern of these two substructures repeats, forming the overall biperiodic structure [45]. A biperiodic structure is constructed from chains of two coupled substructures, each exhibiting periodicity with weak coupling both inside the substructures and at the interfaces. The natural frequencies of a biperiodic structure exhibit a distinctive separation into two distinct sets of natural frequencies.

Fig. 3 shows the equivalent spring-mass-damper model of a biperiodic structure. This structure consists of two periodic substructures with different masses, m_1 and m_2. Substructures are

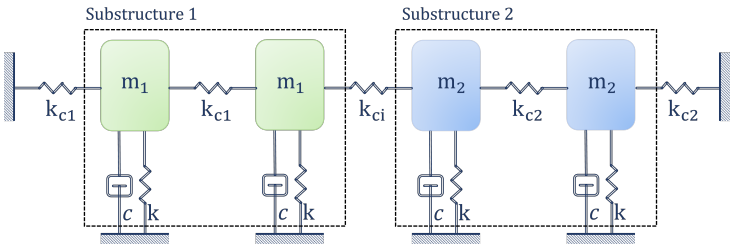

Figure 3: The equivalent spring-mass-damper model of a biperiodic structure.

then coupled together at their interface with a weak coupling stiffness k_{ci} ($\beta_i = \frac{k_{ci}}{k}$).

The first four natural frequencies of the system can be obtained by solving the eigenvalue problem $(\mathbf{K} - \lambda\mathbf{M})\phi = 0$ where $\mathbf{M}$ is the unit mass matrix and $\mathbf{K}$ is the linear stiffness matrix, given by

$$\mathbf{K} = \begin{bmatrix} \omega_0^2(1+\beta_1) & -\omega_0^2\beta_1 & 0 & 0 \\ -\omega_0^2\beta_1 & \omega_0^2(1+\beta_1+\beta_i) & -\omega_0^2\beta_i & 0 \\ 0 & -\omega_0^2\beta_i & \omega_0^2(1+\beta_i+\beta_2) & -\omega_0^2\beta_2 \\ 0 & 0 & \omega_0^2(1+\beta_2) & -\omega_0^2\beta_2 \end{bmatrix} \tag{4}$$

where $\omega_0 = \sqrt{\frac{k}{m_1}}$ is the undamped natural frequency of the system, $\beta_1 = \frac{k_{c1}}{k}$ and $\beta_2 = \frac{k_{c2}}{k}$ are the coupling stiffnesses inside the substructures and $\beta_i = \frac{k_{ci}}{k}$ is the coupling stiffness in the interface between the two substructures. The solutions are distinct real eigenvalues $\lambda_n = \omega_n^2$ for $n = 1, 2, 3, 4$. Table. 1 gives the normalized eigenfrequencies corresponding to two sets of closely spaced modes. The nearness of the normalized eigenfrequencies allows for the exploration of the energy localization phenomenon.

Table 1: Normalized eigenfrequencies of the biperiodic structure with two substructures.

Normalized eigenfrequencies			
1.01	1.02	1.25	1.27

As shown in Fig. 4a, the weakly coupled biperiodic configuration generates two distinct sets of normalized eigenvalues, a direct consequence of its biperiodic architecture. Additionally, the periodicity of the substructures introduces two sets of near-eigenfrequencies in the system. Introduction of mass mistuning to each substructure (Fig. 4b) induces characteristic veering behavior in the eigenfrequency branches, where they approach asymptotically before repelling without intersection. Crucially, the two veering points enable simultaneous mode localization across distinct frequency bands, establishing this approach as a novel variant of multimodal energy harvesting. Furthermore, the concept generalizes to systems comprising p substructures with n oscillators each, yielding p localized vibration modes with corresponding frequency bands containing n clustered eigenfrequencies. This scalable architecture suggests promising potential for broadband vibration energy harvesting applications.

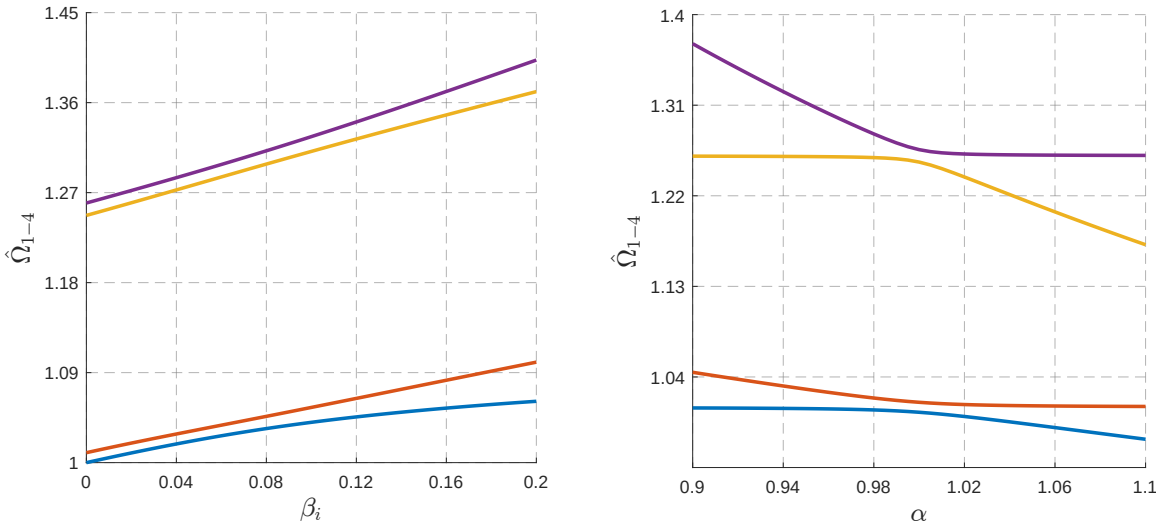

Figure 4: (a) Eigenvalues of the biperiodic structures with the weak coupling between periodic subsystems, (b) Mode veering: normal eigenvalues $\hat{\Omega}_{1-4}$ with mass mistuning in two subsystems in a quasi-biperiodic structure.

2. Formulation of the Optimization problem

The design optimization of the electromagnetic VEH based on periodic and biperiodic structures, illustrated in Fig. 1b, aims to maximize harvested power by introducing mass mistuning into various sets and numbers of subsystems. This optimization procedure targets two conflicting objectives: maximizing the harvested power while minimizing the number of mistuned subsystems. The optimization procedure intends to identify the optimal sets of subsystems for mistuning to obtain an optimal compromise between these two objectives.

The objective functions aim to maximize the harvested power $f_1(y)$, and minimize the number of mistuned subsystems $f_2(y)$ which can be expressed as:

$$f_1(y) = \sum_{j=1}^{N} Z_j R_{load}^j \left(\frac{\omega \delta_{em}}{(R_{load}^j + R_{int})} \right)^2 |X_{max}^j|^2,$$

$$f_2(y) = \sum_{j=1}^{N} Z_j,$$

where y represents all the optimization variables, including Z, α and R_{load}. A mistuning indicator vector $Z = [Z_1, \ldots, Z_j, \ldots, Z_N]$ with a dimension of $1 \times$ N is defined to represent the presence or absence of mistuning in each of the N candidate subsystems. This vector assigns a binary value of 1 to indicate a mistuned subsystem and 0 for a non-mistuned subsystem. A vector of load resistance, $R_{load} = [R_{load}^1, \ldots, R_{load}^j, \ldots, R_{load}^N]$, is defined to identify the optimal load resistance for each subsystem. Optimizing load resistance is essential to achieve maximum energy harvesting. The amount of mistuning for each subsystem is represented by a $1 \times$ N-dimensional vector $\alpha = [\alpha_1, \ldots, \alpha_j, \ldots, \alpha_N]$. This magnitude varies within a specified range to ensure the occurrence of energy localization, where

$$\begin{cases} \alpha_j \neq 1 & \text{the corresponding subsystem is mistuned.} \\ \alpha_j = 1 & \text{the corresponding subsystem is not mistuned.} \end{cases} \quad \text{with } j = 1, \ldots, N.$$

A kinetic energy criterion C_{KE} is introduced to quantify the proportion of kinetic energy in mistuned subsystems relative to the total kinetic energy of the system, as follows:

$$C_{KE} = \frac{\sum_{j=1}^{N} Z_j m_j x_j^2}{\sum_{j=1}^{N} m_j x_j^2}, \tag{5}$$

Bounded by a decision maker value E_{min}, this criterion determines the impact of mistuning on the overall dynamics of kinetic energy.

Based on the defined objective functions and design parameters, this optimization problem can be formulated as follows:

$$\begin{cases} \min\limits_{y} & F(f_1(y), f_2(y)) \\ \text{subject to} & g(y) = -C_{\text{KE}} + E_{\text{min}} \leq 0 \end{cases} \tag{6}$$

where $g(y)$ is a constraint function that ensures that the system operates within the desired range. y is the design variable to achieve the objective functions, which are defined as follows:

$$y = \begin{Bmatrix} Z = [Z_1, \ldots, Z_j, \ldots, Z_N] \\ \alpha = [\alpha_1, \ldots, \alpha_j, \ldots, \alpha_N] \\ R_{load} = [R_{load}^1, \ldots, R_{load}^j, \ldots, R_{load}^N] \end{Bmatrix}. \tag{7}$$

The weighted sum method transforms multiple objective functions into a single objective function by assigning weights to reflect their relative importance [54]. The weighted-sum objective function is formulated as $\min\limits_{y} \sum_{n=1}^{N} w_n f_n(y)$ for $n = 1, 2$. Weights, which must be non-negative and sum to 1, allow the decision-maker to balance conflicting objectives. Different weight combinations yield various Pareto front solutions, representing trade-offs between objectives. Normalization, often by the maximum value of each objective function, ensures a balanced optimization process [55]. This normalization method results in the following formulation of the objective function:

$$\begin{cases} \min\limits_{y} \left(-w_1 \dfrac{f_1(y)}{\max(f_1(\tilde{y}))} + (1 - w_1) \dfrac{f_2(y)}{N} \right), \\ \text{with } \tilde{y} = \begin{Bmatrix} \alpha_j = 1 & \forall j \\ Z_j = 0 & \forall j \\ R_{load}^j = R_{load}^* & \forall j \end{Bmatrix}. \end{cases} \tag{8}$$

where w_1 and $(1 - w_1)$ represent the weights in the two objective functions, respectively. The objective function for maximizing harvested power is normalized by the maximum harvested power from a perfectly periodic system (100% harvested power), which corresponds to the peak total average load power. The objective function for minimizing mistuned subsystems is normalized by the total number of subsystems N.

This optimization problem requires a mixed-integer approach, which effectively optimizes both continuous variables (e.g., mass mistuning value) and integer variables (e.g., the number and location of mistuned subsystems) [56]. The well-known GA optimization algorithm is used in this optimization problem [57]. The GA starts with a population of candidate solutions encoded as chromosomes representing mistuning presence, value, and load resistance. Chromosomes are evaluated and ranked by fitness, with the fittest selected for the next generation. Crossover (rate 0.9) and mutation introduce variation, and the iterative process continues until convergence, yielding the optimal solution.

The design parameters used in this study to implement the optimization procedure are summarized in Table. 2.

Table 2: Constant design parameters of electromagnetic VEH device.

Parameter	**Symbol**	**Value**	**unit**
Linear stiffness	k	105	N/m
Equivalent mass	m	0.65	g
Gap between magnets	d	22×10^{-3}	m
Magnetic coupling stiffness	β	0.012	%
Mechanical damping coefficient	ξ_m	0.16	%
Internal resistance of the coil	R_{int}	17	Ω
Load resistance	R_{load}	25	Ω
Electromechanical coupling coefficient	δ_{em}	0.14	V.s/m

The objective function and optimization design parameters are presented in Table. 3. The kinetic energy criterion requires that the kinetic energy of all mistuned systems be at least 50% of the total system's kinetic energy. The mistuning indicator vector Z identifies which subsystems are mistuned, while small masses (less than 10% of the initial mass) are added to these subsystems to introduce mistuning. The mistuning vector α specifies the amount of mistuning for each subsystem. Optimal load resistance, R^j_{load}, is crucial for maximizing harvested power. The Pareto front analysis helps find a balance between the two objective functions, $f_1(y)$ and $f_2(y)$.

2.1. Optimal design of quasi-periodic VEH devices

The design optimization of electromagnetic VEH with periodic structures is investigated for a device with 20 subsystems. The approach is then extended to harvesters with 100 and 1000 subsystems to evaluate its effectiveness for larger systems.

The optimization of a VEH device with 20 subsystems, illustrated in Fig. 5a, reveals a trade-off between harvested power and the number of mistuned subsystems. The Pareto front shows the trade-off through the weighting parameter w, where $w = 0$ prioritizes minimizing mistuned subsystems while $w = 1$ focuses on maximizing harvested power. Mistuning 4 subsystems allows harvesting 56% of the total energy of a periodic system, increasing to 76% with 8 mistuned subsystems, and 83% with 50% mistuning. Fig. 5b shows that mistuning 25 subsystems among 100 achieves 65% of the total harvested power, while mistuning 40 subsystems enhances power harvesting to over 77%. When half of the subsystems are optimally mistuned, the device yields

Table 3: Objective function and design parameters with associated constraints.

Objective function
$\min_{y} \left(-w \frac{\sum_{j=1}^{N} Z_j R_{\text{load}}^j \left(\frac{\omega \delta_{em}}{(R_{\text{load}}^j + R_{\text{int}})} \right)^2 |X_{\max}^j|^2}{\max(f_1(\tilde{y}))} + (1-w) \frac{\sum_{j=1}^{N} Z_j}{N} \right)$
Design variables with constraints
$y = \left\{ \begin{array}{l} 0.5 \leq C_{KE} \\ Z_j \in \{0,1\}, \text{ for } j = 1, \ldots, N \\ 1 \leq \alpha_j \leq 1.1, \text{ for } j = 1, \ldots, N \\ R_{\text{int}} \leq R_{\text{load}}^j \leq 85, \text{ for } j = 1, \ldots, N \\ 0 \leq w \leq 1 \end{array} \right\}$

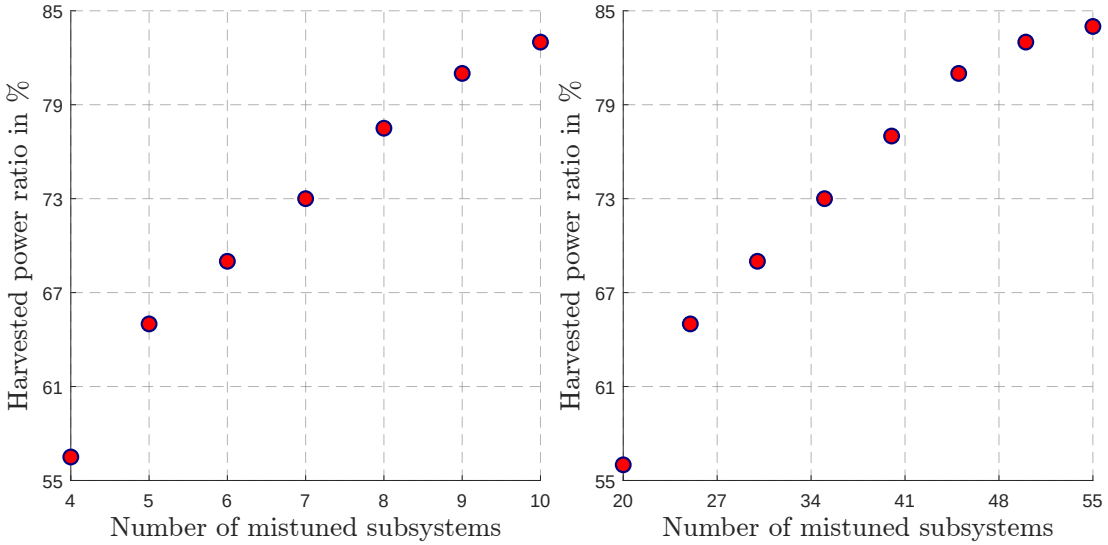

(a) (b)

Figure 5: Pareto front of quasi-periodic VEH devices: harvested power ratio versus the number of mistuned subsystems (a) 20 subsystems (b) 100 subsystems.

84% of the total power. For the 1000-DOF quasi-periodic device, mistuning 315 subsystems leads to harvesting nearly 70% of the total power.

The results reveal a clear relationship between harvested power and the proportion of mistuned subsystems. Table. 4 summarizes the optimized output power for different mistuning numbers in quasi-periodic VEH devices, showing that mistuning 20% of the subsystems can harvest up to 55% of the total energy, mistuning 40% achieves up to 78%, and mistuning 50% reaches up to 84% of the system's total power.

2.2. Optimal design of quasi-biperiodic VEH devices

A biperiodic VEH device is proposed to maximize harvested power over two frequency bandwidths. It is modeled as a spring-mass-damper system, with a basic unit composed of 8 subsystems arranged into two periodic substructures, each containing 4 subsystems with different masses, m_1 and m_2. Weak coupling stiffnesses k_{c1} and k_{c2} within each substructure and k_{ci} at

Table 4: Optimized harvested power ratio for different percentages of mistuned subsystems.

Percentage of mistuned subsystems	20	25	30	35	40	45	50
Percentage of harvested power ratio	56	65	69	73	78	81	84

their interface allow targeting two frequency bandwidths. The unit shown in Fig. 6 is replicated to form the full biperiodic structure.

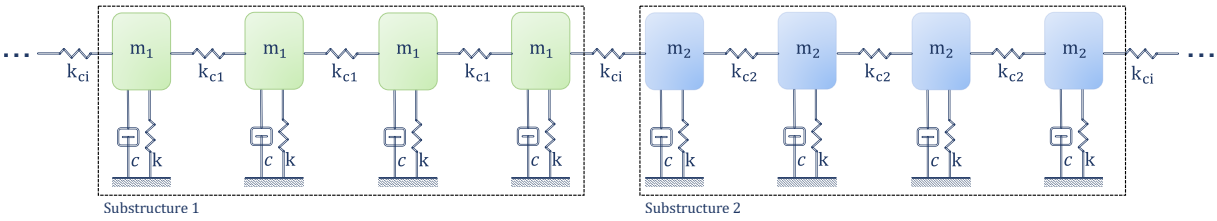

Figure 6: Equivalent spring-mass-damper model of the biperiodic structure's building block.

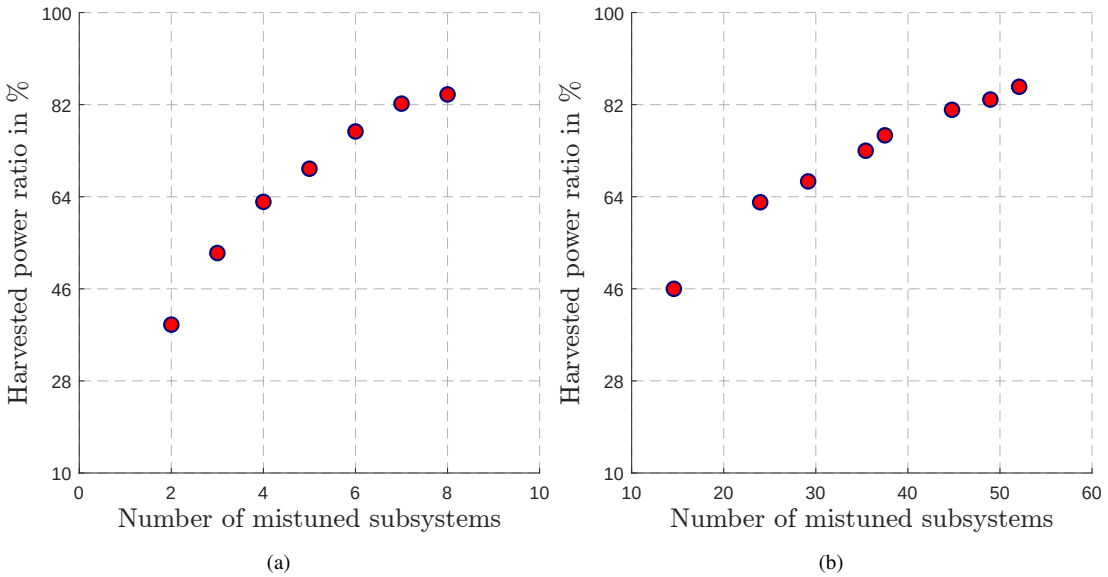

Figure 7: Pareto front of quasi-biperiodic VEH device: harvested power ratio versus the number of mistuned subsystems (a) 16 subsystems (b) 96 subsystems.

Fig. 7a shows optimal mistuning of 4 subsystems achieves 63% of the total harvested power, 6 mistuned subsystems increase this ratio to 77%, and mistuning half the subsystems reaches 84%. Fig. 7b shows that mistuning 24 subsystems yields nearly 63% of the total power, increasing to 76% with 36 mistuned subsystems. Mass mistuning in half of the subsystems further increases the harvested power to over 83% of the total power. The results demonstrate that optimal mistuning of quasi-biperiodic structures, when weakly coupled at the interface between the substructures, offers harvesting performance comparable to optimally mistuned quasi-periodic counterparts. In addition, it offers the advantage of operating across two distinct frequency bandwidths.

3. Experimental validation and discussion

Experimental investigations were conducted to validate the feasibility of the optimization procedure and the numerical findings. Fig. 8a illustrates the designed electromagnetic VEH device, which comprises eight subsystems. The schematic of a single subsystem electromagnetic VEH is shown in Fig. 8b, with a spring and a magnet wrapped by a coil. Each subsystem consists of a spiral-shaped spring, as shown in Fig. 8c. The spiral design maximizes the spring's length within a compact area, effectively reducing its natural frequency. An NdFeB magnet is bonded to a circular stage of 5 *mm* diameter, suspended by two cantilever spring arms.The spiral-shaped springs are anchored to a supporting bar via a frame, with a fixed gap between them to ensure consistent stiffness coupling across successive subsystems. This configuration enables the central stage to vibrate vertically in response to external vibrations. The relative motion between the vibrating magnet stage and the fixed copper coils, also secured to the supporting bar, induces a varying magnetic flux, generating electrical current. The generated electrical energy is dissipated across load resistances.

The designed harvesting device is mounted on the shaker platform, illustrated in Fig. 8d, and subjected to sinusoidal harmonic excitation over a specified frequency range. In a closed-loop circuit, the current generated in the coils is discharged into load resistances. Post-processing of the data is performed by "m+p Vibrunner" pilot software. The output voltage across the load resistances is measured for each coil. Details of the materials and geometric parameters of the magnet and coil are provided in Table 5.

Table 5: Material and geometric parameters of the magnet and coil.

Component	**Parameter**	**Value**
Neodymium Magnet	Magnetization	N45
	Residual magnetic field	1.37 (T)
	Height	6 (*mm*)
	Diameter	3 (mm)
Coil	Internal resistance	17 (Ω)
	Number of turns	73
	Diameter	5 (*mm*)

Fig. 9 shows the frequency response of the harvested power from one subsystem in a periodic VEH with 8 subsystems. The total power of this VEH is the sum of the power of all 8 subsystems. The optimization procedure is applied to the VEH device with 8 subsystems, and the optimal sets of parameters are obtained. These optimal parameters are used in the experimental tests, and the frequency response of harvested power is obtained and compared with the optimization process results.

3.1. Quasi-periodic VEH devices

The optimization procedure is first applied to a VEH device based on a periodic structure with 8 subsystems. For the case with 2 and 4 mistuned subsystems, the optimization process results in the mistuning indicator vector Z, mistuning coefficients α, and load resistances R_{load} shown in Fig. 6. The experimental tests use these optimal parameters, and the corresponding frequency responses are measured.

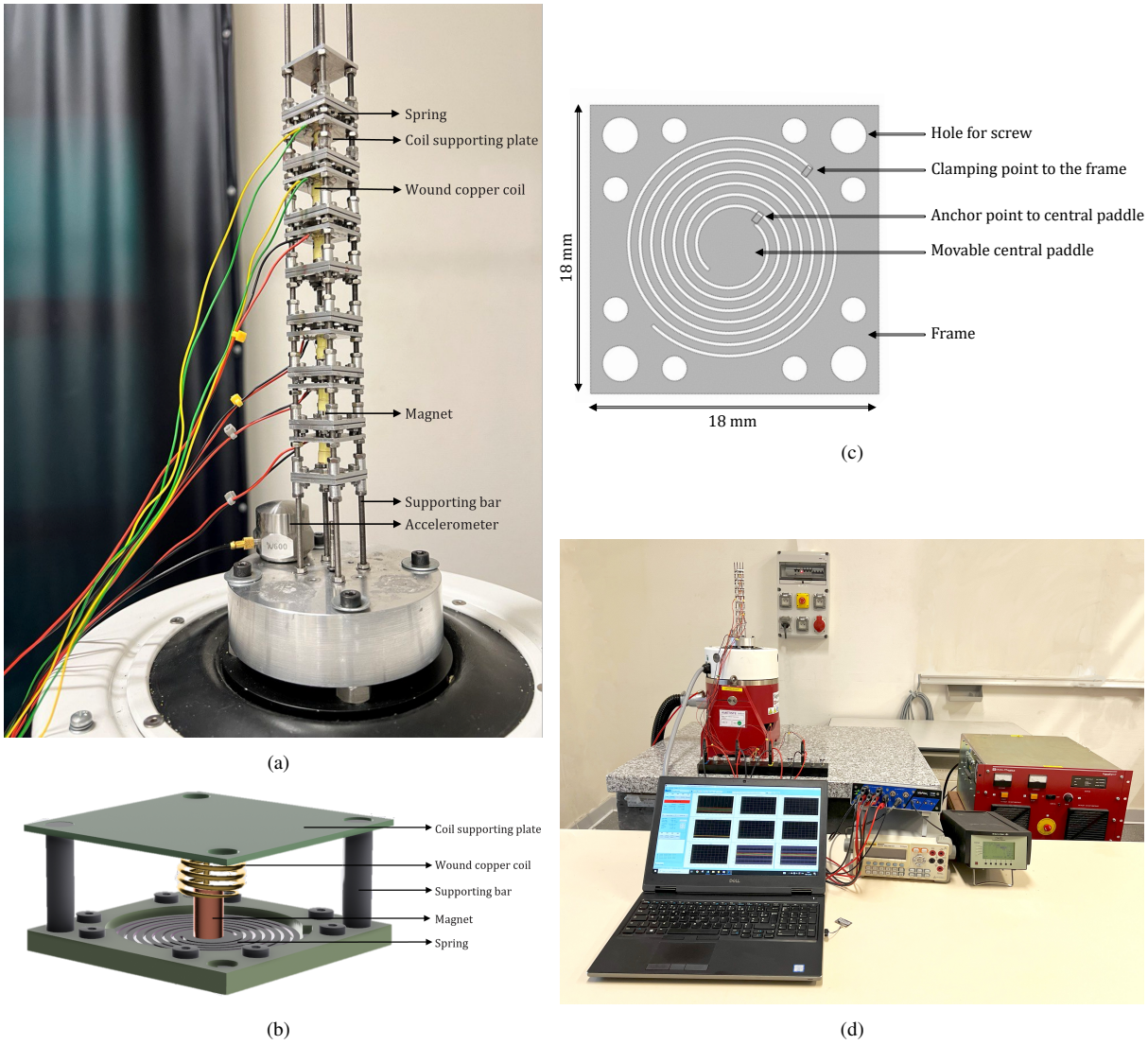

Figure 8: (a) Designed electromagnetic VEH device with 8 subsystems, (b) Schematic of a single-subsystem electromagnetic VEH, (c) The designed spiral-shaped spring, (c) Vibration test setup for energy harvesting.

Mass mistuning is introduced in subsystems 3 and 7, and the harvested power is measured only from these subsystems at an acceleration of 0.1 g at the optimal load resistance value. Fig. 10a shows that the harvested power of these 2 subsystems, exhibits a substantial increase compared to the maximum harvested power before mistuning. While the maximum harvested power in a perfectly periodic system occurs at the resonant frequency, the mistuned system exhibits slight shifts in the resonance peaks due to mode veering and energy localization. For quasi-periodic systems, therefore, the harvested power is defined as the ratio of their peak total power at the shifted frequency to that of the periodic system. To quantify this improvement, the total maximum harvested power from these 2 subsystems is calculated as a percentage of the total harvested power from all 8 subsystems before mistuning. The ratio of harvested power from the mistuned subsystems is 62% of the total energy generated by the VEH device with 8 subsystems.

Mass mistuning is then introduced to 4 specific subsystems, and the power frequency response of these 4 mistuned subsystems is shown in Fig. 10b. However, due to the localization

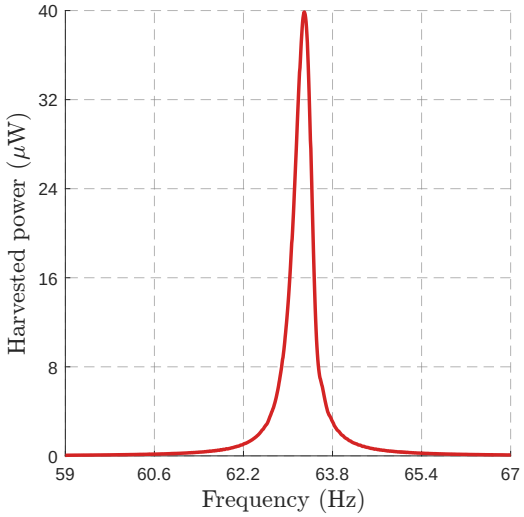

Figure 9: Frequency response of harvested power for one subsystem in the periodic VEH with 8 subsystems at the acceleration of 0.1 g.

of energy in half of the subsystems, the energy localization level at each subsystem is lower compared to the cases with 2 and 3 mistuned subsystems. The energy harvested from the 4 mistuned subsystems accounted for almost 81.5% of the total energy harvested by the 8 subsystems before mistuning.

The harvested power ratio for various numbers of mistuned subsystems is summarized in Fig. 11a. The experimental results align well with the numerical predictions in Fig. 11b, though there's a discrepancy of about 3%. This difference arises due to the system's inherent mistuning and lack of perfect periodicity, which affects energy localization. Additionally, achieving the exact mistuning values from the optimization process is challenging.

3.2. Quasi-biperiodic VEH devices

The optimization process is applied to the VEH device based on a biperiodic structure with 8 subsystems. This is achieved by changing the mass of 4 successive subsystems to 0.8 g. The results reveal that when 2 subsystems undergo optimal mistuning, 65% of the total power of the system can be harvested. Applying the mistuning to 3 subsystems enhances the power ratio to 76%. If half of the harvester's subsystems are mistuned, 84% of the entire system's energy can be harvested. Furthermore, introducing mistuning to 5 subsystems is expected to result in harvesting 89% of the total energy. The design parameters of the harvesters are obtained through the optimization process and reproduced in the experiment validation process. Fig. 7 shows the optimal sets of parameters for 2 and 4 mistuned subsystems. The corresponding frequency of harvested power is measured and shown in Fig. 12a.

Table 6: Optimal design parameters for quasi-periodic VEH device with 2 and 4 mistuned subsystems

Solution for 2 mistuned subsystems	Solution for 4 mistuned subsystems
$Z^* = [0, 0, 1, 0, 0, 0, 1, 0]$	$Z^* = [1, 0, 1, 0, 1, 0, 1, 0]$
$\alpha^* = [1, 1, 1.015, 1, 1, 1, 1.023, 1]$	$\alpha^* = [1.034, 1, 1.013, 1, 1.05, 1, 1.02, 1]$
$R^*_{load} = [-, -, 25, -, -, -, 25, -]$	$R^*_{load} = [25, -, 25, -, 25, -, 25, -]$

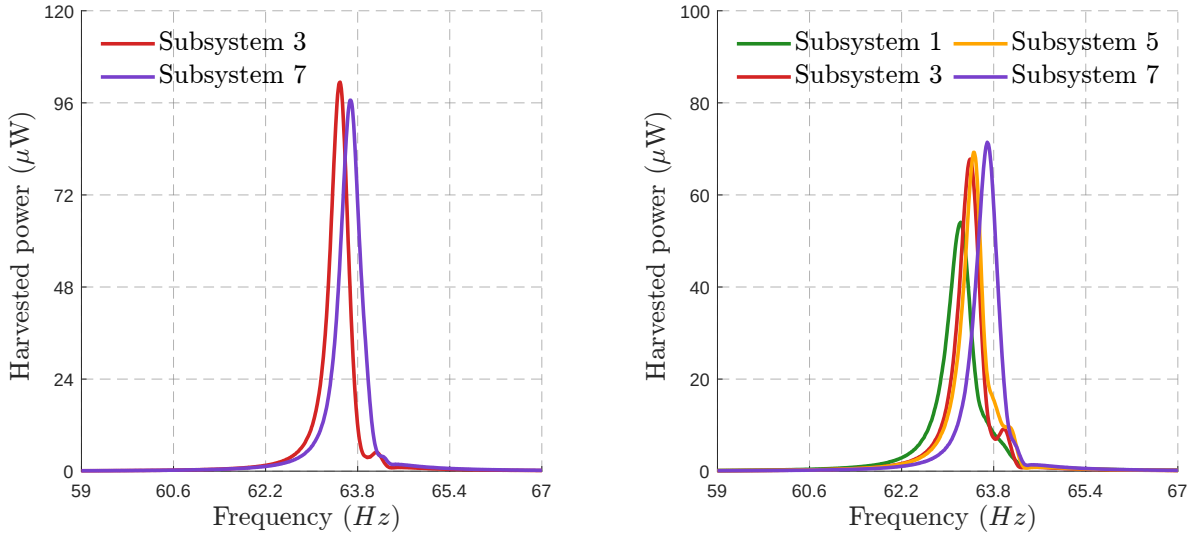

(a) (b)

Figure 10: Power-frequency response of the quasi-periodic VEH with 8 subsystems at the acceleration of 0.1 g with mistuning in (a) 2 subsystems, (b) 4 subsystems.

Table 7: Optimal design parameters for quasi-biperiodic VEH device with 2 and 4 mistuned subsystems

Solution for 2 mistuned subsystems	Solution for 4 mistuned subsystems
$Z^* = [0, 1, 0, 0, 0, 0, 1, 0]$	$Z^* = [1, 0, 1, 0, 1, 0, 1, 0]$
$\alpha^* = [1, 1.013, 1, 1, 1, 1, 1.013, 1]$	$\alpha^* = [1.06, 1, 1.015, 1, 1.05, 1, 1.014, 1]$
$R^*_{load} = [-, 25, -, -, -, -, 25, -]$	$R^*_{load} = [25, -, 25, -, 25, -, 25, -]$

Fig. 12a shows the frequency response of harvested power with 2 mistuned subsystems and it is observed that by adding mistuning the maximum power is considerably increased from the case before mistuning and 62% of the total power before adding mistuning is harvested. As shown, the harvesting is performed on two frequencies and the bandwidth of the system is generally (0.45+0.40 = 0.86) Hz. This is almost twice when harvesting from 2 mistuned subsystems in quasi-periodic harvesters.

To validate the harvested power ratio with the assignment of mistuning to half of the subsystems, the mistuning mass is added to 4 selected subsystems using the parameters presented in Table. 12b. The frequency response of the harvested power is experimentally measured and depicted in Fig.12b. Mass mistuning is added to 2 subsystems within each substructure, targeting the two distinct frequency bandwidths across each substructure. The energy harvested from half of the subsystems is 82% of the biperiodic counterpart without any mistuning.

The harvested power ratio measured experimentally for different numbers of mistuned subsystems is summarized in Fig. 13a. A comparison of the experimental and numerical results (shown in Fig. 13b) reveals a close agreement. This discrepancy can be explained by the inherent imperfections in each subsystem's periodicity before intentional mistuning. Such imperfections can be due to the spiral spring manufacturing process. In the VEH device assembly process, the spiral spring manufacturing process, the boundary conditions, the magnetic coupling stiffness between the subsystems, and the internal resistances of the coil can break the symmetry of the periodic substructures. Although the mistuned subsystem and optimal load

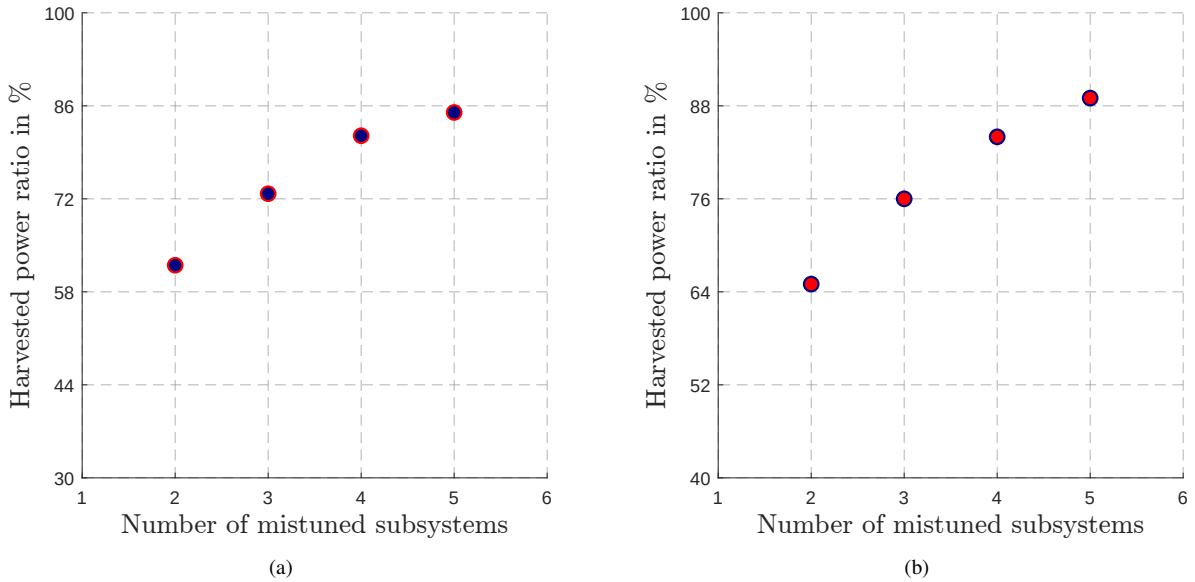

Figure 11: Pareto front of the quasi-periodic VEH device with 8 subsystems: harvested power ratio versus the number of mistuned subsystems: (a) experimental results, (b) numerical results

resistance can be effectively determined and used, accurately replicating the exact mistuning magnitudes in experimental settings is challenging due to practical limitations in scale and precision. Biperiodic structures allow for simultaneous energy harvesting from two frequency bandwidths.

4. Conclusion

This paper proposes an optimized design framework for electromagnetic vibration energy harvesting devices, leveraging weakly coupled periodic and biperiodic structures. The proof of concept based on the optimal design is experimentally validated. This approach permits the maximization of the harvested power and bandwidth by introducing optimal mistuning in terms of mass and location. For periodic structures with 20 and 100 subsystems, mistuning approximately 25% of the subsystems resulted in harvesting 65% of the power compared to a perfectly periodic structure, increasing to 84% when half of the subsystems were mistuned. For biperiodic structures with 16 and 96 subsystems, mistuning approximately 24% yielded 63% of the power from a periodic structure, increasing to 83% with half of the subsystems optimally mistuned. To validate these numerical findings, a proof-of-concept electromagnetic VEH device with eight weakly coupled subsystems was designed and fabricated. The optimization procedure was applied to the device, determining the optimal amount and location of mass mistuning, as well as the optimal load resistance. The numerical and experimental results for both periodic and biperiodic VEH devices showed good agreement. The results also prove that quasi-biperiodic harvesters, which target two distinct frequency bandwidths, enlarge the total harvested bandwidth. This optimization methodology can be applied beyond electromagnetic systems to other transduction methods, broadening the potential for future energy harvesting technologies. Furthermore, the biperiodic concept can be extended to N-periodic structures, where each substructure targets a specific frequency bandwidth, and mistuning leads to energy localization, enabling efficient harvesting within each mistuned subsystem.

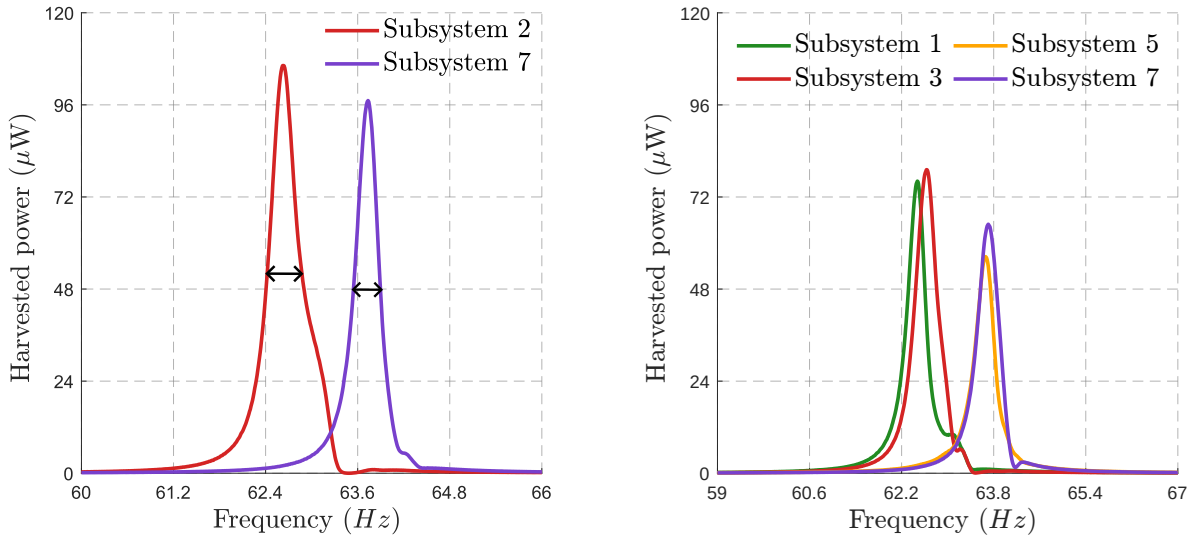

(a) (b)

Figure 12: Power-frequency response of the quasi-biperiodic VEH with 8 subsystems at the acceleration of 0.1 g with mistuning in (a) 2 subsystems, (b) 4 subsystems.

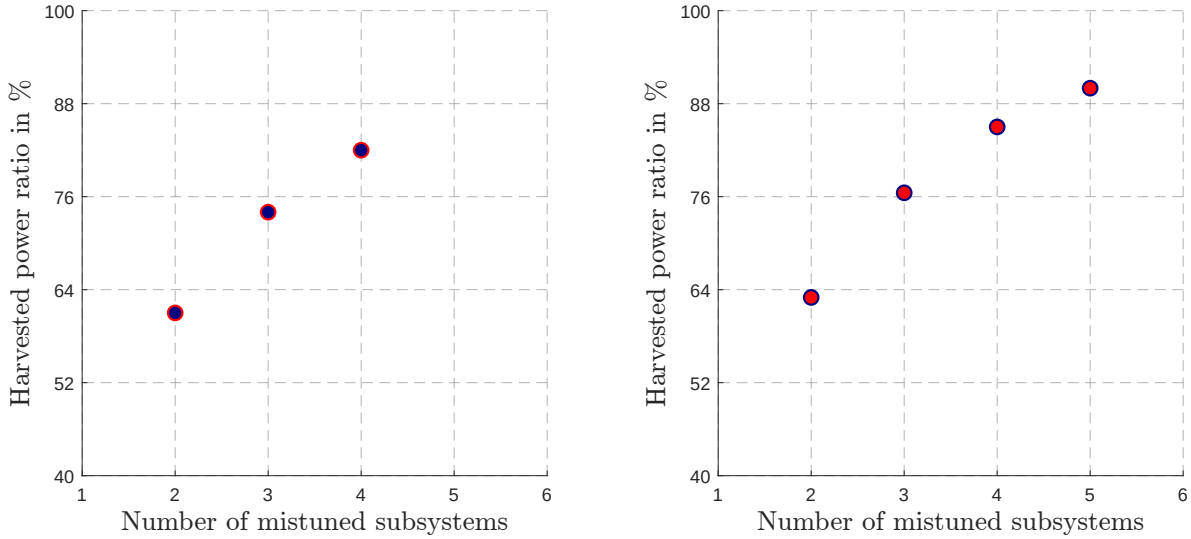

(a) (b)

Figure 13: Pareto front of the quasi-biperiodic VEH device with 8 subsystems: harvested power ratio versus the number of mistuned subsystems: (a) experimental results, (b) numerical results.

Acknowledgments

This work has been supported by the EIPHI Graduate School (contract ”ANR-17-EURE-0002”)

Appendix A. Equations of motion of the proposed VEH device

The governing equations of motion for the vibration energy harvester (VEH) system with N subsystems, subjected to base harmonic excitation $\ddot{X}_g = X_g \sin(\omega t)$, are derived using Newton's 2nd law in matrix form:

$$M\ddot{X} + C\dot{X} + KX = -M[j,j]\ddot{X}_g, \quad j = 1, 2, 3, ..., N, \tag{A.1}$$

where $M = \text{diag}(m, m, ..., m)$ and $C = \text{diag}(c, c, ..., c)$ are the mass and damping matrices, respectively, $X = [x_1(t), x_2(t), ..., x_N(t)]^T$ is the displacement vector, and $M[j,j]$ denotes the diagonal elements of the mass matrix. The stiffness matrix K, incorporating the coupling stiffness k_c between neighboring subsystems, is:

$$K = \begin{bmatrix} k+2k_c & -k_c & 0 & 0 & 0 \\ -k_c & k+2k_c & -k_c & 0 & 0 \\ 0 & \ddots & \ddots & \ddots & 0 \\ 0 & 0 & -k_c & k+2k_c & -k_c \\ 0 & 0 & 0 & -k_c & k+2k_c \end{bmatrix}, \tag{A.2}$$

where k is the stiffness of each subsystem, and k_c is the coupling stiffness due to weak repulsive magnetic forces between adjacent neodymium magnets. To generalize the equations, dimensionless parameters are defined as:

$$\alpha_j = \frac{m_j}{m}, \quad \beta = \frac{k_c}{k}, \quad \omega_0 = \sqrt{\frac{k}{m}}, \tag{A.3}$$

where α_j quantifies the mistuning via the ratio of the j^{th} mass to the reference mass m, β is the electromagnetic coupling coefficient, and ω_0 is the undamped natural frequency. Using these, the dimensionless equation of motion is:

$$\hat{M}\ddot{X} + \hat{C}\dot{X} + \hat{K}X = -\ddot{X}_g, \quad j = 1, 2, 3, ..., N, \tag{A.4}$$

where $\hat{M} = \text{diag}(1, 1, ..., 1)$ is the dimensionless mass matrix, and $\hat{C} = 2\omega_0 \text{diag}(\xi_1, \xi_2, ..., \xi_N)$ is the dimensionless damping matrix, with $\xi_j = \xi_m + \xi_e^j$ combining mechanical and electrical damping coefficients for the j^{th} subsystem. The dimensionless equation can be expressed as:

$$
\begin{bmatrix} 1 & 0 & 0 & 0 & 0 \\ 0 & 1 & 0 & 0 & 0 \\ 0 & 0 & \ddots & 0 & 0 \\ 0 & 0 & 0 & 1 & 0 \\ 0 & 0 & 0 & 0 & 1 \end{bmatrix} \begin{bmatrix} \ddot{x}_1(t) \\ \ddot{x}_2(t) \\ \vdots \\ \ddot{x}_{N-1}(t) \\ \ddot{x}_N(t) \end{bmatrix} + 2\omega_0 \begin{bmatrix} \xi_1 & 0 & 0 & 0 & 0 \\ 0 & \xi_2 & 0 & 0 & 0 \\ 0 & 0 & \ddots & 0 & 0 \\ 0 & 0 & 0 & \xi_{N-1} & 0 \\ 0 & 0 & 0 & 0 & \xi_N \end{bmatrix} \begin{bmatrix} \dot{x}_1(t) \\ \dot{x}_2(t) \\ \vdots \\ \dot{x}_{N-1}(t) \\ \dot{x}_N(t) \end{bmatrix}
$$

$$
+\omega_0^2 \begin{bmatrix} \alpha_1^{-1}(1+2\beta) & -\alpha_1^{-1}\beta & 0 & 0 & 0 \\ -\alpha_2^{-1}\beta & \alpha_2^{-1}(1+2\beta) & -\alpha_2^{-1}\beta & 0 & 0 \\ 0 & \ddots & \ddots & \ddots & 0 \\ 0 & 0 & -\alpha_{N-1}^{-1}\beta & \alpha_{N-1}^{-1}(1+2\beta) & -\alpha_{N-1}^{-1}\beta \\ 0 & 0 & 0 & -\alpha_N^{-1}\beta & \alpha_N^{-1}(1+2\beta) \end{bmatrix} \begin{bmatrix} x_1(t) \\ x_2(t) \\ \vdots \\ x_{N-1}(t) \\ x_N(t) \end{bmatrix}
$$

$$
= -\begin{bmatrix} \ddot{X}_g(t) \\ \ddot{X}_g(t) \\ \vdots \\ \ddot{X}_g(t) \\ \ddot{X}_g(t) \end{bmatrix}. \tag{A.5}
$$

References

[1] S. Chalasani, J. M. Conrad, A survey of energy harvesting sources for embedded systems, in: IEEE SoutheastCon 2008, IEEE, 2008, pp. 442–447.

[2] Z. Zhou, L. Weng, T. Tat, A. Libanori, Z. Lin, L. Ge, J. Yang, J. Chen, Smart insole for robust wearable biomechanical energy harvesting in harsh environments, ACS nano 14 (10) (2020) 14126–14133.

[3] S. A. Graham, S. C. Chandrarathna, H. Patnam, P. Manchi, J.-W. Lee, J. S. Yu, Harsh environment–tolerant and robust triboelectric nanogenerators for mechanical-energy harvesting, sensing, and energy storage in a smart home, Nano Energy 80 (2021) 105547.

[4] S. Khalid, I. Raouf, A. Khan, N. Kim, H. S. Kim, A review of human-powered energy harvesting for smart electronics: recent progress and challenges, International Journal of Precision Engineering and Manufacturing-Green Technology 6 (4) (2019) 821–851.

[5] C. Wei, X. Jing, A comprehensive review on vibration energy harvesting: Modelling and realization, Renewable and Sustainable Energy Reviews 74 (2017) 1–18.

[6] X. Kang, H. Li, J. Wei, J. Qin, X. Zhu, Simultaneous vibration control and energy harvesting for building structures based on electromagnetic technology with negative stiffness inertial amplifier, Structures 77 (2025) 109194. doi:https://doi.org/10.1016/j.istruc.2025.109194.

[7] T.-C. Yuan, J.-Y. Xi, J. Yang, L.-Q. Chen, Dynamic external excitation identification of electromagnetic vibration energy harvesting systems based on improved augmented unscented kalman smoother method, Mechanical Systems and Signal Processing 237 (2025) 113147. doi:https://doi.org/10.1016/j.ymssp.2025.113147.

[8] P. K. Sahoo, S. Roychowdhury, V. Arumuru, Fluid sloshing augmented parametric excitation for enhanced piezoelectric vibration energy harvesting, Sensors and Actuators A: Physical (2025) 117061 doi:https://doi.org/10.1016/j.sna.2025.117061.

[9] D. Ding, J. Fan, H. Wang, G. Jing, Y. Guo, Piezoelectric energy harvesting in railways: Current status and future challenges, Energy Strategy Reviews 61 (2025) 101869. doi:https://doi.org/10.1016/j.esr.2025.101869.

[10] S. Hu, Z. Yuan, R. Li, Z. Cao, H. Zhou, Z. Wu, Z. L. Wang, Vibration-driven triboelectric nanogenerator for vibration attenuation and condition monitoring for transmission lines, Nano letters 22 (13) (2022) 5584–5591.

[11] S. Zhang, Z. Shi, Y. Da, Y. Cui, P. Yu, C. Xue, Y. Zhu, Harvesting multidirectional wind energy based on flow-induced vibration triboelectric nanogenerator with directional tuning mechanism, Sensors and Actuators A: Physical 379 (2024) 115974. doi:https://doi.org/10.1016/j.sna.2024.115974.

[12] A. Hosseinkhani, D. Younesian, P. Eghbali, A. Moayedizadeh, A. Fassih, Sound and vibration energy harvesting for railway applications: A review on linear and nonlinear techniques, Energy Reports 7 (2021) 852–874.

[13] S. P. Beeby, R. N. Torah, M. J. Tudor, P. Glynne-Jones, T. O'Donnell, C. R. Saha, S. Roy, A micro electromagnetic generator for vibration energy harvesting, Journal of Micromechanics and microengineering 17 (7) (2007) 1257.

[14] C. Williams, R. B. Yates, Analysis of a micro-electric generator for microsystems, sensors and actuators A: Physical 52 (1-3) (1996) 8–11.

[15] B. Mann, N. Sims, Energy harvesting from the nonlinear oscillations of magnetic levitation, Journal of sound and vibration 319 (1-2) (2009) 515–530.

[16] F. Cottone, H. Vocca, L. Gammaitoni, Nonlinear energy harvesting, Physical review letters 102 (8) (2009) 080601.

[17] A. Morel, L. Charleux, Q. Demouron, A. Benhemou, D. Gibus, C. Saint-Martin, A. Carré, É. Roux, T. Huguet, A. Badel, Simple analytical models and analysis of bistable vibration energy harvesters, Smart Materials and Structures 31 (10) (2022) 105016.

[18] M. F. Daqaq, R. Masana, A. Erturk, D. Dane Quinn, On the role of nonlinearities in vibratory energy harvesting: a critical review and discussion, Applied Mechanics Reviews 66 (4) (2014).

[19] R. L. Harne, K. Wang, A review of the recent research on vibration energy harvesting via bistable systems, Smart materials and structures 22 (2) (2013) 023001.

[20] T. W. Jensen, A. R. Insinga, J. C. Ehlers, R. Bjørk, The full phase space dynamics of a magnetically levitated electromagnetic vibration harvester, Scientific Reports 11 (1) (2021) 16607.

[21] I. Abed, N. Kacem, N. Bouhaddi, M. L. Bouazizi, Multi-modal vibration energy harvesting approach based on nonlinear oscillator arrays under magnetic levitation, Smart Materials and Structures 25 (2) (2016) 025018.

[22] X. Li, D. Yurchenko, R. Li, X. Feng, B. Yan, K. Yang, Performance and dynamics of a novel bistable vibration energy harvester with appended nonlinear elastic boundary, Mechanical Systems and Signal Processing 185 (2023) 109787.

[23] Y. Jia, A. A. Seshia, An auto-parametrically excited vibration energy harvester, Sensors and Actuators A: Physical 220 (2014) 69–75.

[24] Q. Luo, X. He, S. Jiang, X. Wang, Impact-based electromagnetic energy harvester with high output voltage under low-level excitations, energies 10 (11) (2017) 1848.

[25] M. Wu, J. Zhang, H. Wu, Vibration mitigation and energy harvesting of vibro–impact dielectric elastomer oscillators, International Journal of Mechanical Sciences 265 (2024) 108906.

[26] S. Ghasemi, S. Afrang, G. Rezazadeh, S. Darbasi, B. Sotoudeh, On the mechanical behavior of a wide tunable capacitive mems resonator for low frequency energy harvesting applications, Microsystem Technologies 26 (2020) 2389–2398.

[27] C. Wei, K. Zhang, C. Hu, Y. Wang, H. Taghavifar, X. Jing, A tunable nonlinear vibrational energy harvesting system with scissor-like structure, Mechanical Systems and Signal Processing 125 (2019) 202–214.

[28] C. Hu, X. Wang, Z. Wang, S. Wang, Y. Liu, Y. Li, Electromagnetic vibrational energy harvester with targeted frequency-tuning capability based on magnetic levitation, Nanotechnology and Precision Engineering 7 (4) (2024).

[29] X. Su, J. Xu, X. Chen, S. Sun, D.-G. Lee, B. Zhu, J. M. Baik, S. Hur, S. Fan, H.-C. Song, et al., A piezoelectric-electromagnetic hybrid energy harvester with frequency-up conversion mechanism towards low-frequency-low-intensity applications, Nano Energy 124 (2024) 109447.

[30] Z. Wang, S. Kang, H. Du, P. Feng, W. Wang, A high-performance dual-mode energy harvesting with nonlinear pendulum and speed-amplified mechanisms for low-frequency applications, Energy (2024) 132553.

[31] S. D. Milehsara, N. Kacem, N. Bouhaddi, Enhancing the performance of vibration energy harvesting based on 2: 1: 2 internal resonance in magnetically coupled oscillators, Micromachines 16 (1) (2025) 17.

[32] Y. Pei, Y. Liu, L. Zuo, Multi-resonant electromagnetic shunt in base isolation for vibration damping and energy harvesting, Journal of Sound and Vibration 423 (2018) 1–17.

[33] Y. Shu, K. Wang, T. Chen, H. Pan, Y. Deng, H. Yin, J. Zhou, A quasi-zero-stiffness metastructure for concurrent low-frequency vibration attenuation and energy harvesting, Thin-Walled Structures (2025) 113371.

[34] H. J. Lee, S. I. Kim, D. H. Kim, H. M. Seung, M. Kim, Redesigning finite metasurfaces for enhanced energy harvesting with lead-free (k, na) nbo3 ceramics, Sensors and Actuators A: Physical (2025) 116663.

[35] P. Podder, P. Constantinou, D. Mallick, A. Amann, S. Roy, Magnetic tuning of nonlinear mems electromagnetic vibration energy harvester, Journal of Microelectromechanical Systems 26 (3) (2017) 539–549.

[36] S. Mahmoudi, N. Kacem, N. Bouhaddi, Enhancement of the performance of a hybrid nonlinear vibration energy harvester based on piezoelectric and electromagnetic transductions, Smart Materials and Structures 23 (7) (2014) 075024.

[37] H. Yu, L. Fan, X. Shan, X. Zhang, X. Zhang, C. Hou, T. Xie, A novel multimodal piezoelectric energy harvester with rotating-dof for low-frequency vibration, Energy Conversion and Management 287 (2023) 117106.

[38] D. Li, H. Benaroya, Dynamics of periodic and near-periodic structures (1992).

[39] O. O. Bendiksen, Mode localization phenomena in large space structures, AIAA journal 25 (9) (1987) 1241–1248.

[40] P. W. Anderson, Absence of diffusion in certain random lattices, Physical review 109 (5) (1958) 1492.

[41] Z. Zergoune, N. Kacem, N. Bouhaddi, On the energy localization in weakly coupled oscillators for electromagnetic vibration energy harvesting, Smart Materials and Structures 28 (7) (2019) 07LT02.

[42] P. Malaji, S. Ali, Energy harvesting from near periodic structures, in: Vibration Engineering and Technology of Machinery, Springer, 2015, pp. 411–420.

[43] P. Malaji, S. Ali, Analysis of energy harvesting from multiple pendulums with and without mechanical coupling, The European Physical Journal Special Topics 224 (14-15) (2015) 2823–2838.

[44] K. Aouali, N. Kacem, N. Bouhaddi, E. Mrabet, M. Haddar, Efficient broadband vibration energy harvesting based on tuned non-linearity and energy localization, Smart Materials and Structures 29 (10) (2020) 10LT01.

[45] T. McDaniel, M. Carroll, Dynamics of bi-periodic structures, Journal of Sound and Vibration 81 (3) (1982) 311–335.

[46] M. Wang, W. Wang, Q. Li, Structural optimization of laminated leaf-like piezoelectric wind energy harvesters based on topological method, Advances in Mechanical Engineering 16 (1) (2024) 16878132231224577.

[47] K. Aouali, N. Kacem, N. Bouhaddi, M. Haddar, On the optimization of a multimodal electromagnetic vibration energy harvester using mode localization and nonlinear dynamics, in: Actuators, Vol. 10, MDPI, 2021, p. 25.

[48] S. Li, J. Xu, H. Gao, T. Tao, X. Mei, Safety probability based multi-objective optimization of energy-harvesting suspension system, Energy 209 (2020) 118362.

[49] D. Huang, J. Han, W. Li, H. Deng, S. Zhou, Responses, optimization and prediction of energy harvesters under galloping and base excitations, Communications in Nonlinear Science and Numerical Simulation 119 (2023) 107086.

[50] M. Gao, H. L. Herrera, J. Moon, Optimization of core size and harvested power for magnetic energy harvesters based on cascaded magnetics, in: 2023 IEEE Applied Power Electronics Conference and Exposition (APEC), IEEE, 2023, pp. 2926–2932.

[51] S. Dowlati, N. Kacem, N. Bouhaddi, Optimal design for vibration energy harvesters based on quasi-periodic structures, Physica Scripta 97 (8) (2022) 085212.

[52] S. Dowlati Milesarah, Theses, Université Bourgogne Franche-Comté (Jul. 2024).

[53] ANSYS, Ansys academic research mechanical, release 2024 r2, [Computer software] (2024).

[54] R. T. Marler, J. S. Arora, The weighted sum method for multi-objective optimization: new insights, Structural and multidisciplinary optimization 41 (2010) 853–862.

[55] O. Grodzevich, O. Romanko, Normalization and other topics in multi-objective optimization (2006).

[56] K. Deep, K. P. Singh, M. L. Kansal, C. Mohan, A real coded genetic algorithm for solving integer and mixed integer optimization problems, Applied Mathematics and Computation 212 (2) (2009) 505–518.

[57] S. Sivanandam, S. Deepa, S. Sivanandam, S. Deepa, Genetic algorithms, Springer, 2008.